RSC Advances

ROYAL SOCIETY OF CHEMISTRY

www.rsc.org/advances

Zinc Oxide Microrods and Nanorods: Differential Antibacterial Activity and their Mode of Action against Gram-positive Bacteria

Ilaria Rago,[‖,‡,⊥] *Chandrakanth Reddy Chandraiahgari,*[‖,‡,⊥] *Maria P. Bracciale,*[§] *Giovanni De Bellis,*[‖,‡] *Elena Zanni,*[†] *Mariangela Cestelli Guidi,*[ǂ] *Diego Sali,*[┼] *Alessandra Broggi,*[§] *Claudio Palleschi,*[†,‖] *Maria S. Sarto*[*,‖,‡] and *Daniela Uccelletti,*[*†,‖]

† Department of Biology and Biotechnology "C. Darwin", Sapienza University of Rome, Piazzale Aldo Moro 5, 00185 Rome, Italy

‡ Department of Astronautic, Electrical and Energetic Engineering, Sapienza University of Rome, via Eudossiana 18, Rome 00184, Italy

§ Department of Chemical Engineering, Materials and Environment, Sapienza University of Rome, via Eudossiana 18, Rome 00184, Italy

|| Research Center on Nanotechnology Applied to Engineering of Sapienza (CNIS), SNNLab, Sapienza University of Rome, Piazzale Aldo Moro, 5, Rome 00185, Italy

ǂ Laboratori Nazionali di Frascati - INFN, Via E. Fermi, 40, 00044 Frascati, Rome (Italy).

┼ Bruker Italia Srl Unipersonale, Viale V. Lancetti 43, 20158 Milan (Italy)

Corresponding Authors:

* E-mail: daniela.uccelletti@uniroma1.it; mariasabrina.sarto@uniroma1.it

⊥ These authors contributed equally to the work

Keywords: *Staphylococcus aureus*; Zinc Oxide Microrods; Zinc Oxide Nanorods, FT-IR; antibacterial activity; ICP-MS

Abstract

The development of antibiotic resistance among pathogenic bacteria combined with increased implant-associated infections have determined a great interest towards new bactericidal materials containing various organic and inorganic substances. Among them, Zinc Oxide (ZnO) derived materials have received considerable attention due to their unique antibacterial, antifungal, and UV filtering properties as well as high catalytic and photochemical activities. In the present work, we investigate the antimicrobial properties against two Gram-positive bacteria (*Staphylococcus aureus* and *Bacillus subtilis*) of ZnO microrods (MRs) and nanorods (NRs), produced in bulk quantity through simple and inexpensive methods. We demonstrate that such antimicrobial effect is strongly dependent on the rod size and dose. Scanning electron microscopy analysis revealed that the two investigated microbial types interact differently with the ZnO-MRs and NRs due to their different morphology. This resulted in different outcomes as reported by the respective Colony Forming Unit (CFU) capabilities. Moreover, Fourier Transform Infrared (FT-IR) spectroscopy revealed that changes in cell outer structures, i.e. membrane and exopolysaccharides (EPS), produced by the interaction with the ZnO structures, are responsible for the antimicrobial mechanism without the accumulation of reactive oxygen species. This was further strengthened by the increased survival observed in case of bacterial cells treated in the presence of an osmotic support, like glycerol. In addition, Inductively Coupled Plasma Mass Spectrometry (ICP-MS) analysis showed that reduced cell viability is not correlated strictly to an increased zinc ion release in the suspension. We then concluded that ZnO-NRs have a superior antimicrobial effect against both *S.aureus* and *B.subtilis* at much lower doses when compared to ZnO-MRs. This is mainly due to the smaller diameter of the NR diameter, which promotes surface damaging and protein alteration of the cell wall. Finally, the lack of toxicity and the antimicrobial properties of ZnO-NRs versus *S. aureus,* validated *in vivo* using the nematode *Caenorhabditis elegans* as host infection model, confirms the promising exploitation of ZnO-NRs in biomedical applications.

Introduction

One of the most effective strategies for the prevention of microbial colonization is to develop a functional material with highly antimicrobial properties. Inorganic metal oxides such as TiO_2, MgO, CaO, and ZnO have attracted interest as antimicrobial agents because of their safety, robustness, re-usability, long shelf life and stability.[1,2] Among these, ZnO micro and nano structures are at the cutting edge of research due to their unique optical, electrical and chemical properties as well as their widespread applications.[3] Zinc oxide is a non-toxic and wide band gap (3.37eV) II-VI semiconductor material, exhibiting near-UV emission, optical transparency, electric conductivity and piezoelectricity.[4,5] It has superior durability, greater selectivity and heat resistance as compared to many organic and inorganic materials.[6,7]

It has been shown that ZnO nanoparticles have selective toxicity toward bacteria, and thanks to their biocompatible properties, they have been used as drug delivery scaffolds, cosmetic ingredients, and medical filling materials.[6-8] Moreover, their large surface area is favorable for a marked interaction with microbes. It has been suggested that nano-sized ZnO could be used as an effective fungicide for preserving agricultural products given its excellent antibacterial activity when deposited on cotton fabrics and food.[9] Since ZnO nanoparticles possess antibacterial and antifungal activities at low concentrations with low cytotoxicity, ZnO-based materials are promising as preventive and remedial coatings for various biomedical applications.[9] ZnO particles are reported to exhibit anti-microbial effect on various pathogenic and non-pathogenic bacteria such as *Staphylococcus aureus* and *Escherichia coli*.[10]

S. aureus can infect nearly all host tissues and organs, and staphylococcal disease can vary in severity ranging from skin and soft tissue infections to pneumonia, endocarditis, osteomyelitis, and sepsis.[11] The various immune evasion tactics utilized by *S. aureus* together with the prevalence of antibiotic resistance make this pathogen particularly difficult to treat. Further, the growing spread of multi-drug-resistant bacteria as well as the exploitation of nanomaterials in biomedical applications require an increase in the number of models to be used in these assays. The nematode *Caenorhabditis elegans* is a whole organism model, which is suitable and very convenient to assay toxicity as well as antimicrobial effects of drugs and novel materials. In addition to being a genetically tractable model system, *C. elegans* has a transparent body, which allows the direct observation of infection and gene expression reporters *in vivo* without ethical issues.[12] The lifespan of *C. elegans* on *Escherichia coli*, which is its natural food source, is only about 2 weeks: this makes easy to assess whether pathogens cause a shortening of *C.elegans* lifespan. A wide variety of microbial pathogens have been shown to infect and kill *C. elegans*.[13]

In the literature, the toxicity of aqueous suspension of ZnO nanoparticles is often attributed to interaction of increased levels of reactive oxygen species (ROS), mostly H_2O_2, hydroxyl radicals and singlet oxygen with bacteria.[14,15] An alternative mechanism proposed for antibacterial effect of ZnO nanoparticles is the surface abrasiveness of nanoparticles, leading to cell wall deformation.[6] It was also reported that the release of toxic levels of Zn ions in aqueous suspension of nanoparticles is responsible for cells toxicity.[16]

Moreover, it was reported that the antimicrobial efficacy depends not only on the concentration but also on particles size, shape, and morphology.[17-19] Therefore, it is important to produce nanostructures with narrow size distribution, controlled morphology and purity.

In this work, ZnO microrods (MRs) and nanorods (NRs) are synthesized through solution phase hydrothermal procedure and vapor phase thermal decomposition technique, respectively. Both

synthesis processes are simple, inexpensive and catalyst free. ZnO-MRs as well as ZnO-NRs are produced in bulk quantity with well-defined morphology and limited size distribution, as shown through extensive microscopy investigations. The purity and structural properties of the produced materials were assessed by means of X-Ray Powder Diffraction (XRPD) and by X-Ray Photoelectron Spectroscopy (XPS). Additionally, the potential antimicrobial properties of ZnO-MRs and ZnO-NRs were evaluated against two different Gram-positive bacteria having different shape, namely *S.aureus* and *Bacillus subtilis*. Fourier Transform Infra-Red spectroscopy (FT-IR) was used to reveal changes in the outer cell structure due to the interactions with ZnO-MRs or NRs. Moreover, Inductively Coupled Plasma Mass Spectrometry (ICP-MS) was performed in order to assess zinc ion release versus cell toxicity. Finally, the toxicity and the antimicrobial activity of ZnO-NRs was explored *in vivo* by using the mini host infection model *C.elegans.*

Experimental

Synthesis and characterization of ZnO-MRs and ZnO-NRs

A simple and cost-effective hydrothermal technique with some modifications[20-22] was used for the synthesis of ZnO-MRs. The developed method does not make use of a seed layer, and consists of the steps described below. At first, an aqueous growth solution was prepared by dissolving a 0.02 M equimolar ratio of Zinc Nitrate Hexahydrate (Acros Organics, 98% purity) and Hexamethylenetetramine (Fisher Chemical, 99% purity) in deionized (DI) water. Next, the solution was stirred at 500 rpm for 30 minutes at room temperature and then kept in a laboratory oven at 90°C for 4 ½ h. The growth reaction resulted in a white sedimentation of ZnO-MRs at the bottom of the beaker, which also served as a substrate for the growth. Following the growth, 100 ml DI water were introduced into the beaker in order to rinse the white sedimentation. Successively, a 3 min-bath sonication was carried out to detach the rods grown on the bottom of the beaker and homogenize the suspension. Afterward, the white powder was collected onto an alumina filter disk (Whatman Anopore 47 mm disk, with 20 nm pore size) under vacuum filtration, and subsequently it was dried in oven at 100°C for 15 min.

ZnO-NRs were produced using a thermal decomposition-based process following the work of Chih-Cheng Lin *et al*. (2009)[23]. At first an amount of zinc acetate dihydrate (0.3 g), serving as precursor for the synthesis, was placed between two aluminum foil dishes and then inserted in a tightly closed steel box. This was subsequently positioned in a preheated muffle furnace in air and kept at 300°C for 12 h. ZnO-NRs were thus easily obtained in powder form.

Field Emission Scanning Electron Microscopy (FE-SEM) imaging was performed on the as-produced materials using a Zeiss Auriga SEM, operating at an accelerating voltage of 5 keV (Figures 1-2).

The structural characterizations of the synthesized powders were performed by XRPD with a Bruker D8-Advance X-ray powder diffractometer, using Cu Kα radiation (λ =1.5418Å) in a scanning range 2θ from 20° to 145° with a step size of 0.022° and 1s of counting time at room temperature (RT). Samples were prepared as capillary mounts. Data were evaluated by the Rietveld method using Topas V. 4.2 software.

XPS was performed by pressing the powders onto a pure gold grated foil, which was then placed in a ultra high vacuum (UHV) chamber. XPS and Auger spectra were registered by using an Escalab Mk II spectrometer (VG Scientific) equipped with a 5-channeltron detection system. Photoelectrons were excited by using a standard Al Kα excitation source, whereas spectroscopic data were processed using the Avantage v.5 software by Thermo Fisher Scientific, UK.

Homogeneous suspensions of ZnO-MRs or ZnO-NRs were produced in Phosphate Buffered Saline (PBS) for cell viability tests and in de-ionized (DI) water for Zn ion release evaluation, via probe sonication (Sonics&MaterialsVibracell VCX750) of the aforementioned materials with ultrasound amplitude set at 70%, operating in pulse mode for 20 min. During the sonication, the suspensions were maintained at 15°C through a jacketed beaker, using a water bath circulator. The ZnO-MR or NR suspensions were then readily transferred onto a 50 ml tube, to avoid any sedimentation.

Zn-ion release in suspensions with different concentrations of ZnO-MRs or NRs was analyzed by ICP-MS (Perkin-Elmer SCIEX - ELAN 6100). To this purpose, after sonication the suspension

samples were allowed to settle for 24h at RT. Then, the ZnO rods were removed by two centrifugation steps (for 30 min at 1740 *g*). Supernatants were analyzed after proper dilutions in 1% HNO_3. A Zn ICP standard solution (MERCK, Germany) was employed to set the calibration curves, and a Rh ICP standard solution (BDH, Aristar) was used as an internal standard.

FE-SEM imaging was also performed on the ZnO-MRs and NRs after sonication in DI water, in order to assess any change in size and morphology.

Microbial Strains and Media

Bacillus subtilis PB1831 and *Staphylococcus aureus* ATCC 25923 bacterial strains were used in this study. Bacterial strains were grown in LB broth at 37 °C for 16 h.

Cells viability test

About 5 x 10^7 cells/ml of bacterial strains were incubated in PBS suspensions of ZnO-MRs or ZnO-NRs at different concentrations (from 0.01 to 250 μg/ml) under shaking for 24h at 37°C. Aliquots of samples were withdrawn, diluted and then spread onto LB agar plates. After incubation at 37°C, the capability of the bacteria to form colonies was measured by CFU counting method. Controls were run without ZnO suspensions. For the osmoprotectant test, glycerol (SIGMA) was used at a final concentration of 2% (v/v).

ROS determination

Flow cytometric analysis was used to assess the production of free intracellular radicals as reported.[24] Briefly, 5 x 10^7microbial cells, treated or not for 2 h with ZnO-MR or NR suspensions, were washed with PBS and then incubated with dihydrorhodamine 123 (SIGMA) for 90 min. The analysis was conducted by using a FACS Calibur system (BD Biosciences, San Jose, CA) at a low flow rate with excitation and emission settings at 488 and 525 to 550 nm (filter FL1), respectively.

SEM microscopy imaging of bacterial cells

Bacterial cells were treated with ZnO-MR or NR suspensions at the concentration of 250 μg/ml for 24 h in H_2O_{dd}. Cell suspensions (1.5 x 10^8 cells) were successively processed as described in Zanni et al. 2012.[25] FE-SEM investigations were carried out on treated and un-treated cells using a Zeiss Auriga SEM, operated at different accelerating voltages (varying between 2 and 5 keV) depending on the sample type. Cells were imaged as prepared, without applying any metal coating.

FT-IR

About 5 x 10^8 cells of the bacterial strains were incubated in H_2O_{dd} at 37°C with or without ZnO – MRs (10 μg/ml) or NRs (5μg/ml) under shaking for 90 min. Cells were withdrawn and then fixed with 1 ml of a freshly prepared 4% (v/v) formaldehyde solution. After incubation for 1h in the dark, the samples were washed three times and cells were initially suspended in 15 μl of H_2O_{dd}. The absorbance of bacterial suspensions was spectrophotometrically determined in order to obtain the same cell concentration for all samples. Afterwards, 5μl of these suspensions were drop-cast onto a Zinc Selenide (ZnSe) window and air-dried before the FT-IR analysis. All the Infrared absorption spectra of the microbial replica spots were recorded using a vacuum FT-IR spectrometer (Vertex 70v by Bruker Optics GmbH, residual pressure about 0.1 mbar) in order to perfectly compensate

atmospheric absorptions by water vapour and CO_2. A Liquid Nitrogen cooled MCT detector was used to optimize the signal to noise ratio. Analyses were performed in the typical Mid IR spectral range (4000-600 cm^{-1}). A circular aperture in front of the source of 1 mm was used in order to have a circular spotlight of about 2mm of diameter, covering the drops completely.

For each spectrum an individual background was recorded from blank positions of the IR-plate and 128 interferograms were averaged, at 2 cm^{-1} of spectral resolution.

Mean spectra were the averages of triplicate spectra from at least two independent experiments. The vector-normalized second derivatives of spectra were used to reduce the unavoidable baseline shifts, and to improve the resolution of superimposed bands.

Data collection and spectral calculations were performed using the Opus software package. Water vapor bands were removed by subtracting the water vapor spectra obtained in the blank experiment. The second derivatives of the original spectra were calculated using a 13-point Savitzky-Golay algorithm. During the second derivative process, the amide I band was decomposed to separate overlapping peaks by enhancing spectral resolution. The absorption area and frequency of those bands were obtained from the second derivative spectra to determine the structural changes.

Data are presented as the mean plus or minus the standard deviation (SD) derived from at least three independent experiments. Statistical analysis was performed using Student's t-test; p-values<0.05 were considered significant.

C. elegans survival assay

Nematode survival was evaluated starting from newly hatched L1 larvae and transferred to *E. coli*-Nematode Growth Medium (NGM) plates with suspensions of 5 μg/ml ZnO-NRs. Every second day, animals were transferred to new plates and 200 μl of ZnO suspension was distributed on the NGM plates, before nematodes seeding. Worm death was scored by the absence of touch-provoked movement. For this analysis, 60 worms were used.

In the case of brood size measurement, worms treated with 5 μg/ml ZnO-NR suspensions were allowed to lay eggs at 16°C on NGM supplemented with *E. coli* OP50. Briefly, worms were transferred onto a new bacteria plate every day, and the number of newly hatched larvae was counted. The procedure was repeated for 4 days, until the mother worms stopped laying eggs. Each day the progeny production was recorded and compared with the untreated controls. In both assays, experiments were repeated three times.

For the infection assay, 10 μl of a *S. aureus* overnight culture in Tryptic Soy (TS) broth were spread on 3.5 cm TS agar plates and incubated at 37°C. The plates were then allowed to equilibrate to RT for at least 1 hour before use. Next, 1-day-old adult worms were transferred to agar plates and incubated at 25°C. Nematodes were daily transferred onto fresh *S.aureus*-containing plates and worm mortality was monitored at 24-h intervals. Statistical analysis was performed by using the Kaplan-Meier method provided by GraphPad Prism Software. Two independent experiments were performed.

Results

ZnO-MRs were synthesized through a hydrothermal technique. FE-SEM analysis of these structures revealed a definite hexagonal cross-section, with dimensions ranging between 200 nm and 500 nm in diameter and 2-4 μm in lengths. ZnO-MRs resulted generally aggregated in cross- or star-like clusters (Figure 1). During the probe sonication step, most of the cluster-like structures were split apart to make mono-dispersed MRs with a shorter length ranging between 1-2 μm, and unaltered diameter (Figure 1 C, D).

ZnO-NRs were synthesized through a thermal decomposition technique. FE-SEM analysis revealed that as-grown NRs have diameter ranging between 20 nm and 40 nm and length up to 4μm (Figure 2 A,B). Moreover, it was observed that after probe sonication ZnO-NRs were reduced in length down to an average value of 500 nm, but they were not modified significantly in diameter size (Figure 2 C,D).

The crystalline structure of ZnO-MRs and NRs was investigated by XRPD. The recorded diffraction patterns of the synthesized materials were in agreement with the published Joint Committee on Powder Diffraction Standards (JCPDS) card 036-1451 of ZnO. Diffraction peaks of impurity were not detected in both MRs and NRs, indicating that the synthesized materials are of high-purity. Cell parameters of the NRs resulted smaller than those of MRs and were match with the reference synchrotron X-ray powder diffraction standard of zincite[26] (Table 1). The dimensions of the anisotropic coherency domains were in good agreement with the diameter and length of the rod, as measured by electron microscopy.

The chemical composition and purity of MR and NR powders were investigated by XPS analysis. In both powders, zinc resulted in its Zn^{2+} chemical state, i.e. in the form of oxide,[27] as witnessed by their corresponding Binding Energy (B.E.) and Auger parameters values (Table 2).

Afterwards, the interaction between both types of ZnO structures with Gram-positive bacteria was investigated. Specifically, a cell viability assay was carried out on *B. subtilis* bacteria after a 24h-treatment with these materials. The antibacterial potential was explored by treating cells with different concentrations of ZnO-MRs and NRs (Figure 3 A). The obtained results indicated that exposure to ZnO-MRs and NRs led to a significant antibacterial activity against the tested cells in a dose-dependent manner. In the case of bacterial cells treated with 5 μg/ml ZnO-MR suspension, a viability of 35%, when compared with the untreated cells, was recorded. Moreover, a mortality rate of 93% was achieved at the highest concentration of 250 μg/ml (Figure 3A). Almost identical results were obtained when MR-suspensions were not probe-sonicated (data not shown). In the case of bacterial cells treated with ZnO-NRs, a striking antibacterial activity was observed even at very low concentrations. In fact, only the 17% of *B. subtilis* cells survived after the treatment at 0.01 μg /ml and less than 3% of viability was reported at the concentration of 1 μg/ml. We did not observed any residual cell survival when the ZnO-NR concentration was increased up to 5 μg/ml (Figure 3 A).

Next, FE-SEM analysis was performed in order to investigate how MRs and NRs interact with bacterial cell surfaces. The micrographs (Figure 3 B, C, and D) gave evidence that *B.subtilis* adhered tightly to ZnO-MRs and NRs, and that bacterial cells became crumpled in the presence of both types of ZnO structures. In addition, it appeared that ZnO-NRs acted as needles penetrating the bacterial cell wall. The stronger interactions between bacterial cells and ZnO-NRs when compared with ZnO-MRs (as evidenced through FE-SEM observations), correlate with the higher antimicrobial activity of the nanostructures over their micro counterparts.

In the case of the *S.aureus* strain, a relevant antibacterial activity of ZnO-MRs and NRs was observed. Similarly to the case of *B. subtilis*, NRs showed the highest killing potential as compared to MRs (Figure 4A). In fact, only 22% of viability was reported at the highest MRs concentration (250 μg/ml) with respect to the control. Instead, in the case of NRs, more than 97% of cells died after the treatment with 1 μg/ml ZnO-NR suspension. Finally, we did not observe any cell survival at higher concentrations (from 25 up to 250 μg/ml).

Unlike *B. subtilis* bacteria, FE-SEM analysis of treated *S.aureus* cells showed that microrods adhered only partially to the cell surface (Figure 4C), probably due to their quasi-spherical shape. Instead, ZnO-NRs penetrated the *S.aureus* cell wall, similarly to the case of the rod-shape bacteria *B.subtilis* (Figure 4D).

In order to assess if the antimicrobial properties of MRs and NRs could be related to the presence of zinc ions (Zn^{2+}) released in the suspension, the ICP-MS technique was used. The measurement of the Zn^{2+} release was performed in the supernatants, obtained upon centrifugation of the produced suspensions. At the concentrations corresponding to the maximum bactericidal action (250 μg/ml for MRs and 25 μg/ml for NRs), the Zn^{2+} release from MRs was 60% higher than the one recorded from NRs (Table 3). However, in suspensions with the same concentration of MRs or NRs (i.e. at 5 and 25 μg/ml), the released amount of zinc ions was higher in the case of NRs. Nevertheless, it must be mentioned that in ZnO-NR suspension at 1 μg/ml, the Zn^{2+} content was very low (i.e. 0.567 μg/ml), even if the antimicrobial effect against both types of investigated bacterial cells was relevant.

Next, reactive oxygen species (ROS) accumulation was evaluated by cytofluorimetric analysis in order to investigate whether ZnO structures could cause oxidative stress in Gram-positive bacteria. No ROS production was observed in ZnO-treated cells, suggested that the interaction with both MRs and NRs did not induce oxidative stress in both microrganisms (data not shown).

FT-IR spectroscopy was used in order to assess whether the relevant morphological modifications observed by FE-SEM on the surface of ZnO-treated cells, were associated to alterations of the bacterial cell structure and surface components.[28] In order to detect the early changes in the bacterial cells during the treatments, FT-IR was carried out after 90 min of treatment. Specifically, it was chosen the concentration at which almost 95% of the cells were viable at the analyzed time (data not shown), i.e. 10 μg/ml in the case of MRs and 5μg/ml for NRs. Initially, the FT-IR spectra from untreated cells were examined. Absorption bands representative of various functional groups of polysaccharides and proteins, which are characteristics of bacterial cells, were found (Figure S1 and Table S1). Bacterial IR spectra were further analyzed in the amide I (1600-1700 cm^{-1}) and polysaccharides (1200-900 cm^{-1}) regions to extract information on protein secondary structure and potential changes due to exposure to ZnO structures. The 2nd derivative spectra of *S.aureus* cells (Figure S1 and Table S2) resulted in three distinct regions, as described below.

The first region, between 1800 and 1500 cm^{-1}, is dominated by the conformation-sensitive amide I and amide II bands (around 1656 and 1543 cm^{-1}),which are the intense bands in the spectra of nearly all bacterial samples and reflects quantitative and qualitative relationships between the various secondary structures adopted by the polypeptide chains.[29-31] The second derivative of the amide I band enhances the spectral resolution: the bands around 1658 $cm^{-1}$are associated with α-helices and the bands at 1638 $cm^{-1}$are ascribed to β-sheets. The *S. aureus* cells showed a higher band intensity of the α-helix region than the β-sheet one, indicating an elevated content of α-helices

in the overall cell proteins. The exposure of bacteria to ZnO structures decreased the ratio relative to the β-sheets and α-helices band areas, demonstrating changes in the proteins structure (Figure 5).

It was possible to observe also weak bands, which can be assigned to amino acid side-chain vibrations, near 1496 cm^{-1} (phenylalanine), 1515 cm^{-1} (tyrosine) and between 1585 and 1570 cm^{-1} (aspartate and glutamate carboxylate stretching). Notably, the exposure to ZnO-MRs increased the intensity of the tyrosine band, the most resolved band in this region, while the cells treated with the NRs did not show this variation (Figure 5).

In the second region, around 1230 cm^{-1}, we observed superimposed bands typical of different >P=O double bond asymmetric stretching vibrations of phosphodiester, free phosphate and monoester phosphate functional groups. Treated cells showed a strikingly reduction of the band near 1239 cm^{-1} with respect to the control ones, most probably due to the phosphodiester functional groups of DNA/RNA polysaccharide backbone structures (Figure 5).

The third spectral region, between 1200 and 900 cm^{-1}, is generally dominated by the symmetric stretching vibration of PO_2^- groups in nucleic acids and a complex sequence of peaks mainly due to C-O-C and C-O-P stretching vibrations of various oligo- and polysaccharides. The 2nd derivative FT-IR spectra revealed distinct differences in absorbance intensity, which indicated the variation in quantity of individual components present in the exopolysaccharide (EPS) of *S.aureus* cells upon ZnO structures exposure. The EPS from control showed a stretching frequency at 1093 cm^{-1} of C-O-C wagging frequency that represents the C-O-C group of polysaccharides.[32] The area of this band decreased in the spectra derived from treated bacteria (Figure 5). Therefore, the overall changes in this region confirm alterations in bacterial polysaccharide structures upon interaction between ZnO rods and the cell surface.

A viability assay was performed in the presence of an osmoprotectant, such as glycerol,[33] in order to support the hypothesis that one of the killing mechanism is related to alterations of the cell wall produced by the interaction with ZnO-MRs or NRs. The use of glycerol improved remarkably *S. aureus* cell survival upon ZnO treatment. Notably, bacterial cells treated with MRs showed a 60% increase in the viability when glycerol was added. In the case of NRs the viability increase was only of 30% (Figure 6).

Taking advantage of the mini host infection model *C.elegans,* the toxicity and the antimicrobial properties of ZnO-NRs were explored also *in vivo*. Control experiments on possible toxic or genotoxic effects of nanorods, were firstly run with wild type animals fed with *E.coli* OP50 (normal food). In this case, lifespan and progeny production of nematodes, treated with such nanomaterial, did not show any difference with respect to the case of untreated animals, demonstrating the lack of ZnO-NR induced toxicity (data not shown). Finally, animals infected with *S.aureus* were treated with a 5 μg/ml ZnO-NR suspension, which was added to the growth medium. In this case, the survival of the infected animals increased along all the lifespan (Figure 7).

Discussion

Various methods are reported in the literature for the fabrication of ZnO micro and nanostructures such as hydrothermal synthesis, thermal decomposition, chemical vapor deposition, sol–gel, spray pyrolysis, and precipitation.[34-38]

Herein, we have synthesized ZnO-MRs and NRs in bulk quantity with narrow size distribution through simple and inexpensive techniques, which can provide both qualitative and quantitative support for their commercial applications. Chemical and structural purity and crystallinity of the synthesized ZnO rods were assessed through XPS and XRPD, respectively. Promising antimicrobial properties of as-synthesized ZnO-MRs and NRs have been explored. Both types of ZnO rods displayed a relevant antimicrobial activity, although NRs were more effective than MRs, even at very low concentrations. These findings are in agreement with data from Raghupathi and coworkers (2011), who have demonstrated that ZnO nanomaterial exerts its antibacterial potential in a size-dependent manner.[39] Currently, ZnO is listed as a safe material by FDA (Food and Drug Administration, USA).[40] Early works have demonstrated that antimicrobial textiles can be prepared using ZnO coatings on cotton fabrics.[41] It has also been reported the antibacterial activity of PVC films coated by ZnO powder against food borne pathogens.[42]

Previous studies suggested that the mechanism of ZnO toxicity may be related to its photosensitivity and production of ROS under specific wavelength high-intensity light irradiation; therefore, nanomaterials can indirectly damage cell membranes through lipid peroxidation, as a means of ROS accumulation. Alterations and damage of the cell wall were observed in the bacteria exposed to MgO- and ZnO-derived materials.[43,44] However, in our study, ROS generation was not detected. On the other hand, the tested microrganisms displayed cellular injuries after ZnO exposure. Recently, in agreement with our observations, it was found that the toxicity exerted by MgO and ZnO nanoparticles on bacterial cells was related to membrane damages, while oxidative stress and ROS production were not present on those cells.[45,46]Moreover, the amount of released zinc ions, measured by ICP-MS technique, cannot account for the main toxicity mechanism exerted by either ZnO-MRs or ZnO-NRs. In fact, the most concentrated MR suspension (250 μg/ml) that released the greatest amount of free Zn^{2+} (10.126 μg/ml) led to a mortality rate in *S.aureus* cells limited to 70% with respect to untreated cells. On the contrary, the NR dispersion at 25 μg/ml, having a lower content of zinc ions (i.e. 6.3 μg/ml), induced a 100% mortality on the treated cells. Actually, even the 1 μg/ml ZnO-NR suspension, which released a very low amount of Zn^{2+} (i.e. 0.567 μg/ml), had an almost complete killing effect (98.5%) over the treated cells. Hence, it can be hypothesized that free Zn^{2+} contributes only partially to the antimicrobial activity, which probably results from the mechanical interaction between ZnO rods and the bacterial surface. As discussed in the following, such conclusion was assessed by FT-IR analysis and viability tests in the presence of glycerol.

On the other hand, NRs exhibited a higher Zn^{2+} release than MRs, when comparing suspensions at the same concentrations (5 and 25 μg/ml). This can be ascribed to the larger specific surface area (SSA) of NRs as compared to their micro counterparts. In fact, the SSA values, estimated from FE-SEM observations, following a previous study by Jang *et al.*,[47] resulted to be ~20 m^2/g and ~2 m^2/g for NRs and MRs, respectively. It follows that ZnO-NRs expose a larger contact area to the environment.

The hypothesis that ZnO-MRs and NRs exposure produces cell damages was supported by FE-SEM and FT-IR spectroscopy. More specifically, FE-SEM images revealed that both type of ZnO rods

induced damages more severely on *B. subtilis* cells than on *S. aureus*, in agreement with the survival data. This suggests that cell morphology plays a relevant role in the efficacy of the antimicrobial activity of ZnO rods.

S. aureus has the ability to grow in a wide range of temperatures, pH and salt concentrations allowing its survival in many environments, causing health problems.[48,11] Its exposed surface consists of multiple layers of two insoluble networked carbohydrates, teichoic acid and peptidoglycan, constituting the cell wall.[49] FT-IR analysis revealed that the cytotoxicity-related changes depend probably on damages to proteins and phospholipids. In fact, the beta-alpha ratio decreased after mixing the *S. aureus* cells with the ZnO-MRs or NRs, in agreement with a previous work on *B. subtilis* and *E. coli* cells treated with metal oxide nanoparticles.[50] The different types of proteins on the cell surface have important roles in cell physiological activities. When proteins adhere to particles or solid surfaces, their secondary structures may change and partial protein unfolding may occur.[51-53] It is possible that the β-sheet structure in the proteins is reduced because of protein unfolding or changes in the carbonyl group due to the hydrogen-bonding environment, thereby decreasing the sensitivity of β-sheet structure to infrared light.

Moreover, such alterations observed by FT-IR spectroscopy, could produce DNA damages, since several proteins are needed for DNA stability and replication.

Actually, *S.aureus* cells treatment with ZnO-MRs or NRs can damage the EPS, which plays a relevant role in nutrient acquisition and in the protection of the bacterial cells from environmental stresses, and can affect cell physiological activities. The EPS damage was highlighted by the increased amount of tyrosine observed in cells treated with ZnO-MRs, as a result of proteins denaturation. In fact, autophosphorylation on a C-terminal tyrosine rich motif of tyrosine-kinases, which are present in a large array of bacterial species, has been shown to play a crucial role in the biosynthesis or in the export of capsular polysaccharide.[54] However, it cannot be ruled out the possibility that the cells could also try to increase the signaling to *de novo* synthesis of EPS to reinforce their barrier. Since the increased tyrosine amount was not observed after ZnO-NRs treatment, a different effect of these structures on EPS functionality should be hypothesized. It is possible to speculate that NR interactions do not enable the EPS compensatory response to the cell wall damages, as it happens in the case of MR-treatment. This results in a stronger antimicrobial property of the ZnO-NRs compared to the MRs.

The phospholipid membrane is also protected by cell surface biopolymers and usually does not interact with the particles or surfaces during normal bacterial adhesion processes in the environment. However, ZnO rods could disturb the phospholipids chemical structure by altering the EPS, and leading to the highly disordered conformation of the alkane chain as suggested by the IR spectra. These changes can disrupt the membrane homeostasis causing the leakage of the periplasm, especially in the case of the NR-treatment that resulted in a higher mortality rate with respect to the MR one. Since numerous important cell physiological activities occur in the periplasm, damage to phospholipid structure can lead to bacterial cell death.

It has been reported that ZnO nanoparticles may distort and damage bacterial cell membrane, resulting in a leakage of intracellular contents and eventually the death of bacterial cells.[55] However, there is still a current lack of exact information regarding the interaction of this kind of materials with the bacterial cells. The FT-IR analysis highlighted herein for the first time the specific chemical changes occurring to the cells of *S.aureus* treated with ZnO-MRs and NRs.

Based on the results of our study, it is possible to speculate that ZnO structures cause cell wall defects resulting in a defective osmotic balance, as supported by FE-SEM observations and FT-IR analysis, being the NRs more effective in the damage with respect to MRs. The experiments performed in the presence of an osmotic support seem to confirm this hypothesis.

Taking advantage of the tractability and simplicity of *C. elegans* as an intact host model, we also assessed the antimicrobial effect of ZnO-NRs, as well as their lack of toxicity, in the context of a whole organism. The primary route and major site of infection for *S. aureus* in a *C. elegans* model is the intestine.[56] *S. aureus* accumulates and distends the worm intestinal lumen thereby killing the host. The infected animals, treated with ZnO-NRs, showed an increased survival compared to infected untreated nematodes.

Conclusion

In the present work, we investigated the antimicrobial properties of ZnO-MRs and NRs against two Gram-positive bacteria. ZnO-MRs and NRs were produced in bulk quantity through hydrothermal and thermal decomposition techniques, respectively. These were characterized by a well controlled size distribution, which was achieved thanks to the proper setting of the synthesis parameters. The adopted production techniques are simple, inexpensive and do not make use of a seed layer. FE-SEM analysis demonstrated that the as-synthesized MRs are characterized by a definite hexagonal wurzite structure, with dimensions ranging between 200 nm and 500 nm in diameter and 2-4 μm in lengths, while the NRs have a diameter in the range 20-40 nm and length up to 4 μm. XPS and XRPD analysis revealed the high purity and crystallinity of both ZnO rod types.

The results of the viability tests performed on *S.aureus* and *B.subtilis* demonstrated the superior dose-dependent antibacterial activity of ZnO-NRs with respect to ZnO-MRs. It was also demonstrated that such antimicrobial effect is mainly originated by the direct interaction of the ZnO rods with the cell walls. In fact, neither ROS production nor the amount of released Zn^{2+} from the materials could account for this activity. On the contrary, FE-SEM characterizations highlighted that the exposure of these bacteria to ZnO rods resulted in significant morphological alterations and mechanical damage of the bacterial surface, especially in the case of *B.subtilis*. Moreover, for the first time, FT-IR spectra analysis of *S. aureus* cells indicated that the toxic-related mechanisms of the ZnO structures account for EPS changes. The increased cell viability observed in the presence of an osmoprotectant like glycerol further supports our hypothesis that the main killing mechanism is related to the cell surface damages induced by the ZnO rods.

Finally, the exploitation of a simple yet multicellular organism such as *C. elegans* allowed the *in vivo* assessment of the ZnO nanorods antimicrobial activity.

Based on this data, we can conclude that ZnO-NRs show a great potential in biomedical applications due to their strong antimicrobial activity against bacteria pathogens like *S.aureus*, and to the lack of toxicity with respect to a whole organism like *C.elegans*.

Acknowledgements

We thank Prof. P. Ballirano (Sapienza-University of Rome) for helpful analysis and comments on XRPD analyses, Mr. S. K. Balijepalli and Dr. S. Kaciulis (CNR-ISMN, Monterotondo, Rome) for XPS analyses and Mr.F. Castelli for technical assistance. We are also in debt to Dr. G. Armiento and Dr. M. Montereali (ENEA-UTPRA, Rome) for ICP-MS analysis.

This work was funded by "Ateneo 2013" -Sapienza University of Rome and in part by Regione Lazio within the Project ULS003 "NANOLAB: A laboratory for the development of multifunctional innovative micro/nanostructured materials and devices". Additional funding was provided by Ministry of Education, University and Research (MIUR) through a CINECA National Research Program (Prot. n. 0042358). EZ was the recipient of a Pasteur Institute, Cenci Bolognetti Foundation "Teresa Ariaudo" fellowship.

References

1 L. K. Adams, D. Y. Lyon and P. J. Alvarez, *Water Res,* 2006, **40**, 3527.

2 J. Sawai, *J Microbiol Methods,* 2003, **54,** 177.

3 J. B. Baxter and E.S. Aydil, *Appl. Phys. Lett,* 2005, **86**, 53114.

4 J. S. Wellings, N.B. Chaure, S. N. Heavens and I. M. Dharmadasa, *Thin Solid Films,* 2007**, 516**, 3893.

5 M. G. Ma, Y. J. Zhu, G. F. Cheng and Y. H. Huang, *Materials Letters*, 2008, **62**, 507.

6 N. Padmavathy and R. Vijayaraghavan, *Science and Technology Advanced Materials,* 2008, **9**, 1.

7 L. He, Y. Liu, A. Mustapha and M. Lin, *Microbiological Research*, 2011, **166**, 207.

8 K. Matsuyama, N. Ihsan, K. Irie, K. Mishima, T. Okuyama and H. Muto, *J Colloid Interface Sci*., 2013, **399**,19.

9 S. Gunalana, R. Sivaraja and V. Rajendranb, *Progress in Natural Science: Materials International,* 2012, **22**, 693.

10 P. Singh and A. Nanda*, Journal of Chemical and Pharmaceutical Research*, 2013, **5**, 457.

11 G. L. Archer, *Clin. Infect. Dis.*, 1998, **26**, 1179

12 J. E. Irazoqui, J. M. Urbach and F. M. Ausubel, *Nat Rev Immunol,* 2010, **10**, 47.

13 K. M. Balla and E. R. Troemel, *Cell Microbiol,* 2013*,* **15**, 1313.

14 J. Sawai, E. Kawada, F. Kanou, H. Igarashi, A. Hashimoto, T. Kokugan and M. Shimizu, *J. Chem. Eng. Jpn.,*1996, **29**, 627.

15 A. Lipovsky, Z. Tzitrinovich, H. Friedmann, G. Applerot, A. Gedanken and R. Lubart, *J. Phys. Chem. C*, 2009, **113**, 15997.

16 Y. Y. Kao, Y. C. Chen, T. J. Cheng, Y. M. Chiung and P. S. Liu, *Toxicol. Sci.,* 2012, **125**, 462.

17 K. R. Raghupathi, R. T. Koodali and A. C. Manna, *Langmuir,* 2011, **27,** 4020.

18 J. Pasquet, Y. Chevalierb, E. Couvala, D. Bouviera, G. Noizeta, C. Morlièrea and M.A. Bolzinger, *International Journal of Pharmaceutics,* 2013, **460**, 92.

19 L. K. Adams, Delina Y. Lyon and P. J. J. Alvarez, *Water Research*, 2006, **40**, 3527.

20 D. Polsongkrama, P. Chamninok, S. Pukird, L. Chowb, O. Lupan, G. Chai, H. Khallaf, S. Park and A. Schulte, Physica B., 2008, **403**, 3713.

21 S. Xu, C. Lao, B. Weintraub and Z. L. Wang, *J. Mater. Res*., 2008, **23**, 2072.

22 G. Amin, M. O. Sandberg, A. Zainelabdin, S. Zaman, O. Nur and M. Willander, *J. Mater Sci*., 2012, **47**, 4726.

23 C.-C. Lin and Y. Y. Li, *Materials Chemistry and Physics*, 2009, **113**, 334.

24 M. Olivi, E. Zanni, G. De Bellis, C. Talora, M. S. Sarto, C. Palleschi, E. Flahaut, M. Monthioux, S. Rapino, D. Uccelletti and S. Fiorito, *Nanoscale*, 2013, **5**, 9023.

25 E. Zanni, G. De Bellis, M. P. Bracciale, A. Broggi, M. L. Santarelli, M. S. Sarto, C. Palleschi and D. Uccelletti, *Nanoletters*, 2012, **12**, 2740.

26 Y.-I. Kim, K. Page and R. Seshadri, *Applied Physics Letters*, 2007, **90**, 101904.

27 S. Kaciulis, L. Pandolfi, E. Comini, G. Faglia, M. Ferroni, G. Sberveglieri, S. Kandasamy, M. Shafiei and W. Wlodarski, *Surf. Interface Anal*., 2008, **40**, 575.

28 R. Davis and L.J. Mauer, *International Journal of Food Microbiology*, 2011, **150**, 140.

29 J. Buijs and W. Norde, *Langmuir,* 1996, **12**, 1605.

30 D. Naumann, C. P. Schultz and D. Helm, in *Infrared Spectroscopy of Biomolecules,* (Eds: H. H. Mantsch, D. Chapman, John Wiley and Sons), New York, USA, 1996, 279.

31 H. Torii and M. Tasumi, in *Infrared Spectroscopy of Biomolecules,* (Eds: H. H. Mantsch, D. Chapman, John Wiley and Sons), New York, USA, 1996, 1.

32 G. Sheng and H. Yu, C. Wang, *Appl. Microbiol. Biotechnol.*, 2006, **73**, 204.

33 O. Vilhelmsson and K. J. Miller, *Journal of Food Protection.*, 2002*,* **65**, 1008.

34 R. Ayouchi, D. Leinen, F. Martin, M. Gabas, E. Dalchiele and J. R. Ramos-Barrad, *Thin Solid Films*, 2003, **426**, 68.

35 Z.M. Dang, L.Z. Fan, S.J. Zhao and C.W. Nan, *Mater. Sci. Eng. B*, 2003, **99**, 386.

36 Z. Fu, Z. Wang, B. Yang, Y. Yang, H. Yan and L. Xia, *Mater. Lett.*, 2007, **61**, 4832.

37 P. Hari, M. Baumer, W.D. Tennyson and L.A. Bumm, *J. Non-Cryst. Solids,* 2008, **354**, 2843.

38 M.H. Habibi and M. Khaledi-Sardashti, *J. Iran.Chem. Soc*., 2008, **5**, 603.

39 K. R. Raghupathi, R. T. Koodali and A. C. Manna, *Langmuir,* 2011, **27,** 4020.

40 A. Emamifar, M. Kadivar and M. Shahedi, S. S. Zad, *Food Science and Emerging Technologies,* 2010, **11**, 742.

41 R. Rajendran, C. Balakumar, H. A. M. Ahammed, S. Jayakumar, K. Vaideki and E. M. Rajesh, *International Journal of Engineering, Science and Technology,*2010, **2**, 202.

42 X. Li, Y. Xing, Y. Jiang, Y. Ding and W. Li, *International Journal of Food Science and Technology*, 2009, **44**, 2161.

43 P. K. Stoimenov, R. L. Klinger, G. L. Marchin and K. J. Klabunde, *Langmuir*, 2002, **18**, 6679.

44 R. Brayner, R. Ferrari-Lliou, N. Brivois, S. Djediat, M. F. Bebedetti and F. Fievet, *Nano Lett.*, 2006, **6**, 866.

45 Y. H. Leung , A. M. C. Ng , X. Xu , Z. vbhen , L. A. Gethings , M. T. Wong , C. M. N. Chan , M. Y. Guo , Y. H. Ng , A. B. Djurisic , P.K. H. Lee , W. K.Chan , L. H. Yu , D. L. Phillips , A. P. Y. Ma and F. C. C. Leung, *Small,* 2014, **10**, 1171.

46 Y. H. Leung, C. M. N. Chan, A. M. C. Ng, H. T. Chan, M. W. L. Chiang, A. B. Djurisic, Y. H. Ng,W. Y. Jim, M. Y. Guo, F. C. C. Leung,W.K. Chan and D. T. W. Au, *Nanotechnology*, 2012, **23,** 475703.

47 E. S. Jang, J.-H. Won, S.-J. Hwang, and J.-H. Choy. *Adv. Mater*. 2006, **18**, 3309.

48 M. Schmitt, U. Schuler-Schmid and W. Schmidt-Lorenz, *International Journal of Food Microbiology*, 1990, **11**, 1.

49 J. R. Weber, P. Moreillon and E. I. Tuomanen, *Current opinion in Immunology,* 2003, **15**, 408.

50 W. Jiang, K. Yang, R. W. Vachet and B. Xing, *Langmuir*, 2010, **26**, 18071.

51 A. A. Vertegel, R. W. Siegel and J. S. Dordick, *Langmuir*, 2004, **20**, 6800.

52 M. A. Strehle, P. Rosch, R. Petry, A. Hauck, R. Thull and W. Kieferc, *J. Phys. Chem. Chem. Phys.*, 2004, **6**, 5232.

53 X. Wu and G. Narsimhan, *Langmuir*, 2008, **24**, 4989.

54 C. Grangeasse, S. Nessler and I. Mijakovic, *Philos. Trans. R. Soc. Lond. B Biol. Sci*., 2012, **367**, 2640.

55 Y. Liu, L. He, A. Mustapha, H. Li, Z. Q. Hu and M. Lin, *J.Appl.Microbiol*. 2009, **107**, 1193.

56 C. D. Sifri, J. Begun, F. M. Ausubel and S. B. Calderwood. *Infect. Immun.*, 2003, **71**, 2208.

Figure legends

Figure 1. FE-SEM images of hydrothermally grown ZnO-MRs as obtained (A, B) and after the probe sonication in DI water (C, D), showing typical dimensions ranging between 200 nm – 500 nm in diameter, and lengths to 1μm - 2 μm after sonication.

Figure 2. FE-SEM images of ZnO-NRs as obtained (A, B) and after probe sonication in DI water (C, D), showing typical dimensions ranging between 20nm - 40nm in diameter, and lengths reduced to ~500 nm after sonication.

Figure 3. Antibacterial activity of ZnO dispersions against *B. subtilis*. (A) Concentration–dependent antibacterial activities of ZnO-MRs and NRs against bacteria cells. Loss of cell viability rate was obtained by colony counting method. Error bars represent the standard deviation; $P<0.01$. Scanning electron microscopy of (B) *B. subtilis* bacteria incubated in H_2O_{dd} for 24h in comparison with (C) microrods- and (D) nanorods-treated cells. (Scale bar = 200 nm).

Figure 4. Antibacterial activity of ZnO dispersions against *S. aureus*. (A) Concentration–dependent antibacterial activities of ZnO-MRs and NRs against bacteria cells. Loss of cell viability rate was obtained by colony counting method. Error bars represent the standard deviation; $P<0.05$. Scanning electron microscopy of (B) *S. aureus* bacteria incubated in H_2O_{dd} for 24h in comparison with (C) microrods- and (D) nanorods-treated cells. (Scale bar = 200 nm).

Figure 5. FT-IR data of *S.aureus* cells treated with microrods (10 μg/ml) or nanorods (5 μg/ml) for 90 min. Band area values, calculated from 2nd derivative spectra, are expressed as fold changes in comparison with untreated cells (UT) set as 1. Reported values represent β sheets/α helices ratio (1638/1658 cm^{-1}), tyrosine (1515 cm^{-1}), DNA (1238 cm^{-1}) and polysaccharides (1093 cm^{-1}). Data are derived from at least three independent experiments; p-values are at least less than 0.05, except for the data marked NS (not significant).

Figure 6. Cell viability analysis of ZnO-treated bacteria in the presence of an osmoprotective molecule. Evaluation of colonies formation for *S. aureus* cells treated with microrods (250 μg/ml) or nanorods (10 μg/ml) for 24h together with glycerol (2%). Error bars represent the standard deviation; $P<0.05$.

Figure 7. Kaplan-Meier survival plot of *S. aureus*-infected worms treated with PBS (UT) or ZnO nanorods suspension (5 μg/ml). Worm mortality was monitored at 24-hour intervals. The graph presents the average of three plates per condition, each with 15 to 20 animals per plate. **P< 0.01 (log rank 0.0012) Data are representative of two biological replicates.

Table 1. XRPD basal (*a*) and axial (*c*) lattice parameters of ZnO-MRs and ZnO-NRs (standard deviation in brackets), and of standard ZnO.

ZnO structure	*a* (nm)	*c* (nm)
MRs	0.325071(4)	0.520775(7)
NRs	0.324979(2)	0.520637(4)
Standard[26]	0.325030(9)	0.52072(2)

Table 2. XPS and Auger spectra peak positions of ZnO-MRs and ZnO-NRs.

	ZnO-MRs	ZnO-NRs
$Zn2p_{3/2}$ B. E. (eV)	1021.4	1021.5
Zn LMM K.E. (eV)	988.5	988.5
α (eV) (B.E.+K.E.)	2009.9	2010

Table 3. Zn^{+2} concentration measured by ICP-MS in suspensions of ZnO-NRs or ZnO-MRs at different concentrations in H_2O_{dd}.

Type of ZnO dispersed structures	Suspension concentration (µg/ml)	Concentration of $[Zn^{+2}]$ (µg/ml)
NR	1	0.567
NR	5	2.580
NR	25	6.321
MR	5	1.324
MR	25	2.190
MR	250	10.126

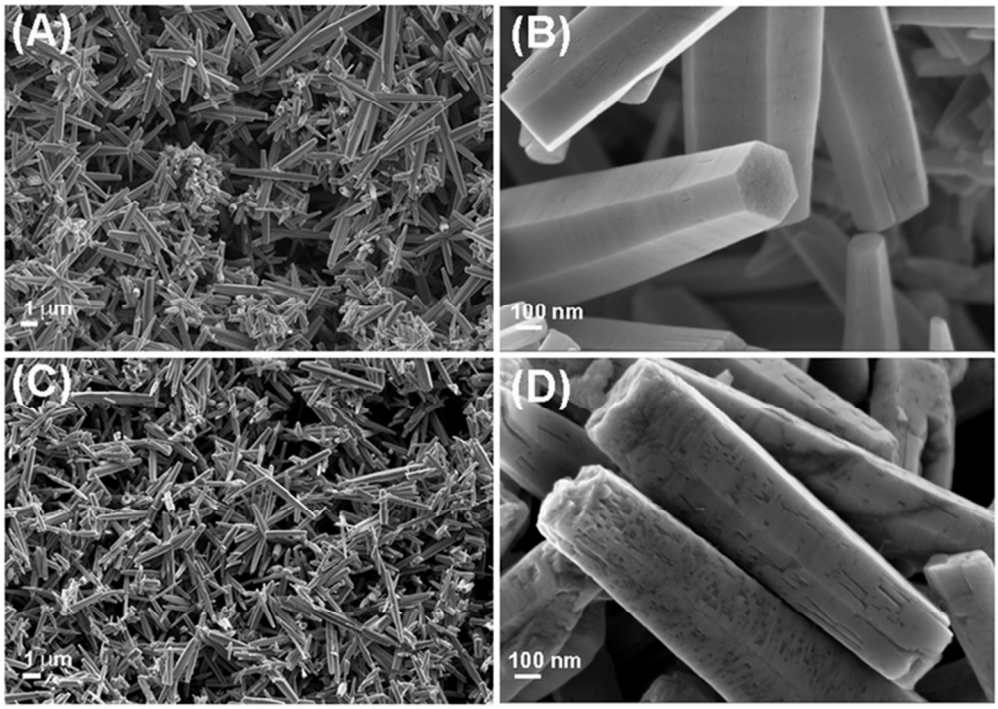

Figure 1. FE-SEM images of hydrothermally grown ZnO-MRs as obtained (A, B) and after the probe sonication in DI water (C, D), showing typical dimensions ranging between 200 nm – 500 nm in diameter, and lengths to 1µm - 2 µm after sonication.
65x53mm (300 x 300 DPI)

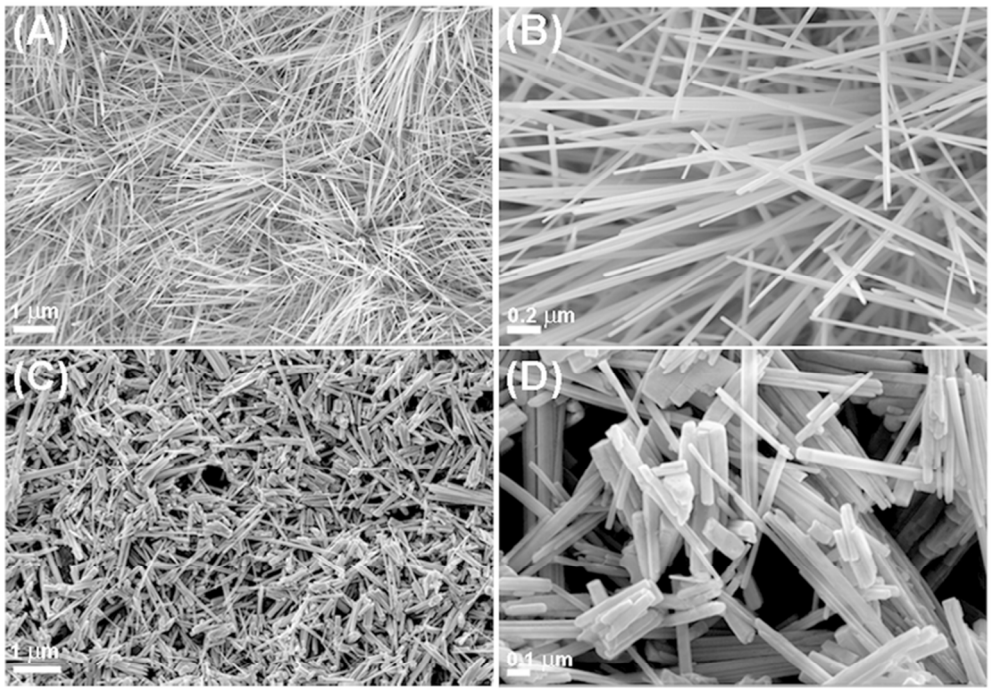

Figure 2. FE-SEM images of ZnO-NRs as obtained (A, B) and after probe sonication in DI water (C, D), showing typical dimensions ranging between 20nm - 40nm in diameter, and lengths reduced to ~500 nm after sonication.
69x60mm (300 x 300 DPI)

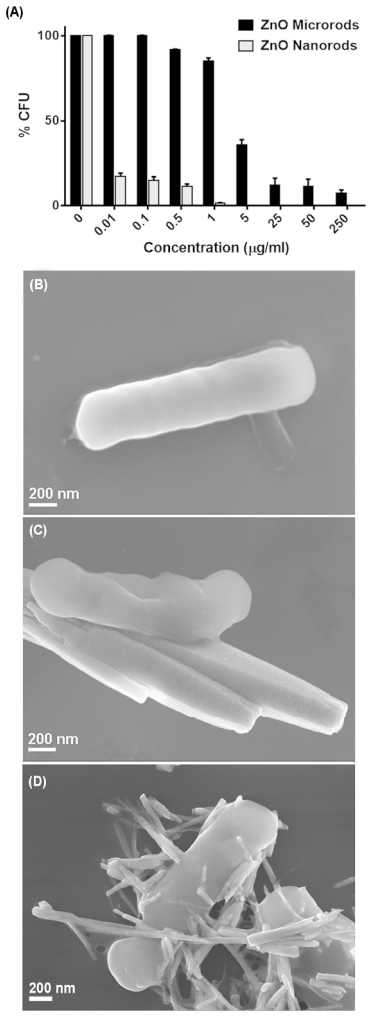

Figure 3. Antibacterial activity of ZnO dispersions against *B. subtilis*. (A) Concentration–dependent antibacterial activities of ZnO-MRs and NRs against bacteria cells. Loss of cell viability rate was obtained by colony counting method. Error bars represent the standard deviation; P<0.01. Scanning electron microscopy of (B) *B. subtilis* bacteria incubated in H_2O_{dd} for 24h in comparison with (C) microrods- and (D) nanorods-treated cells. (Scale bar = 200 nm).
250x781mm (300 x 300 DPI)

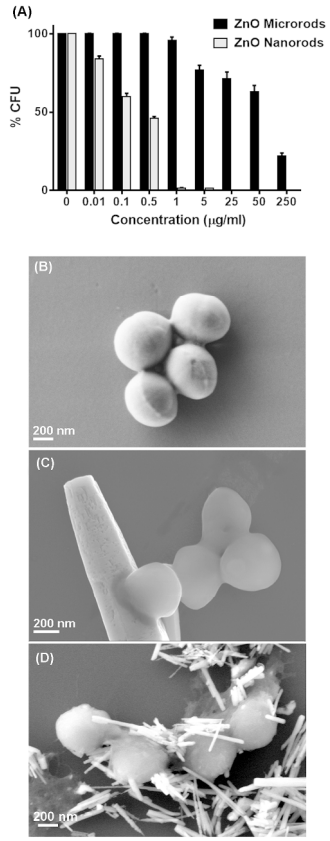

Figure 4. Antibacterial activity of ZnO dispersions against *S. aureus*. (A) Concentration–dependent antibacterial activities of ZnO-MRs and NRs against bacteria cells. Loss of cell viability rate was obtained by colony counting method. Error bars represent the standard deviation; $P<0.05$. Scanning electron microscopy of (B) *S. aureus* bacteria incubated in H_2O_{dd} for 24h in comparison with (C) microrods- and (D) nanorods-treated cells. (Scale bar = 200 nm).
299x1124mm (300 x 300 DPI)

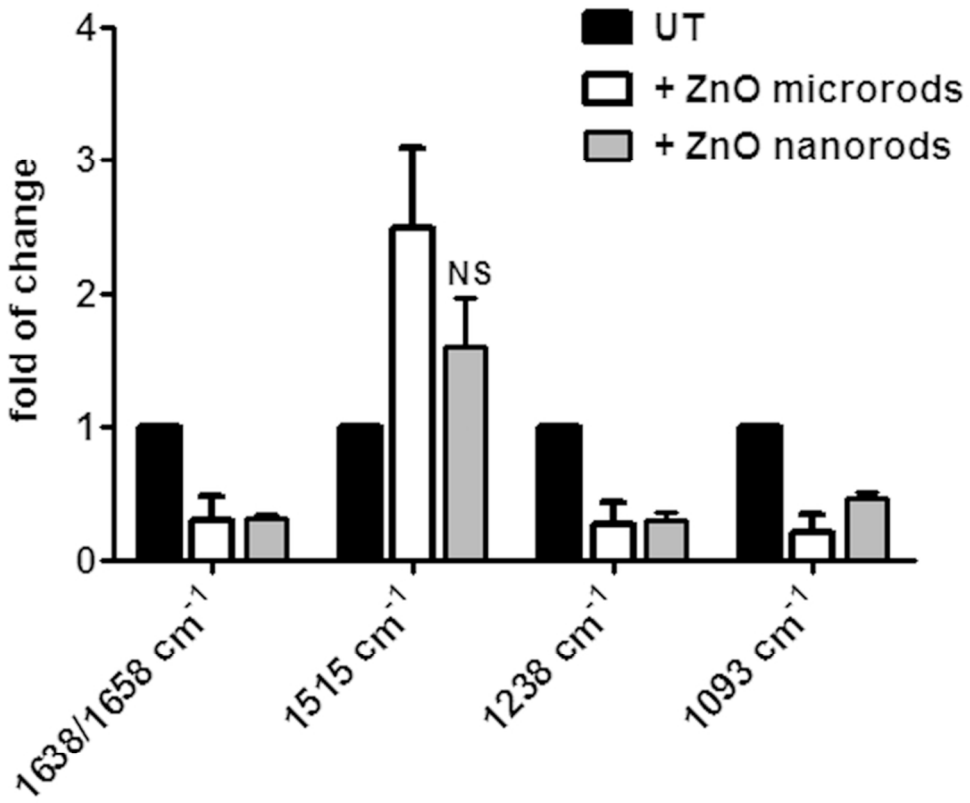

Figure 5. FT-IR data of *S.aureus* cells treated with microrods (10 μg/ml) or nanorods (5 μg/ml) for 90 min. Band area values, calculated from 2nd derivative spectra, are expressed as fold changes in comparison with untreated cells (UT) set as 1. Reported values represent β sheets/α helices ratio (1638/1658 cm^{-1}), tyrosine (1515 cm^{-1}), DNA (1238 cm^{-1}) and polysaccharides (1093 cm^{-1}). Data are derived from at least three independent experiments; p-values are at least less than 0.05, except for the data marked NS (not significant).
78x77mm (300 x 300 DPI)

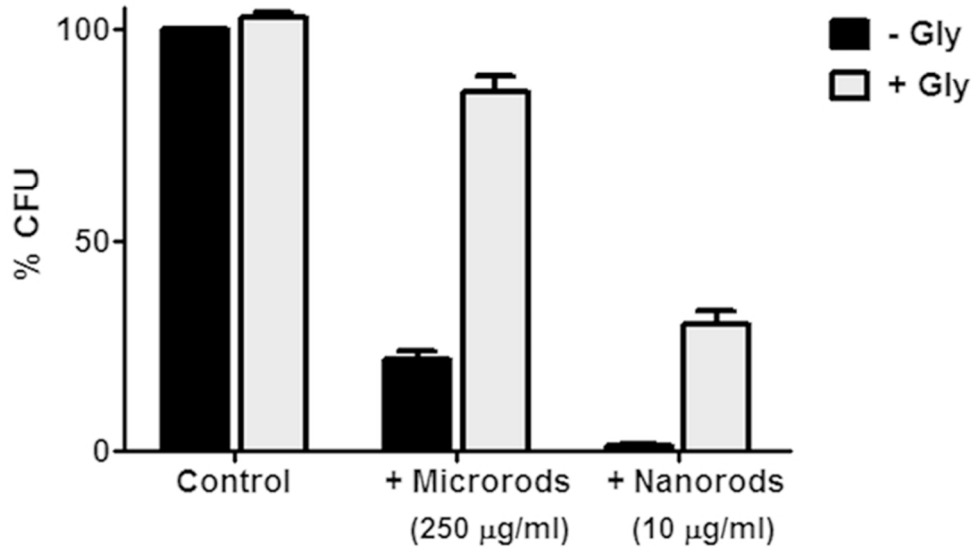

Figure 6. Cell viability analysis of ZnO-treated bacteria in the presence of an osmoprotective molecule. Evaluation of colonies formation for *S. aureus* cells treated with microrods (250 μg/ml) or nanorods (10 μg/ml) for 24h together with glycerol (2%). Error bars represent the standard deviation; $P<0.05$.
67x56mm (300 x 300 DPI)

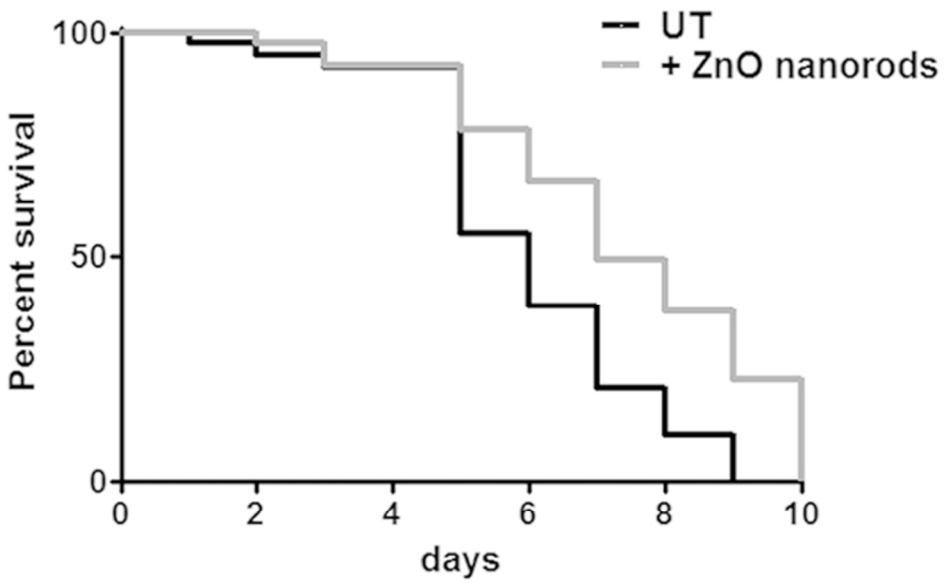

Figure 7. Kaplan-Meier survival plot of *S. aureus*-infected worms treated with PBS (UT) or ZnO nanorods suspension (5 µg/ml). Worm mortality was monitored at 24-hour intervals. The graph presents the average of three plates per condition, each with 15 to 20 animals per plate. **P< 0.01 (log rank 0.0012) Data are representative of two biological replicates.
65x54mm (300 x 300 DPI)

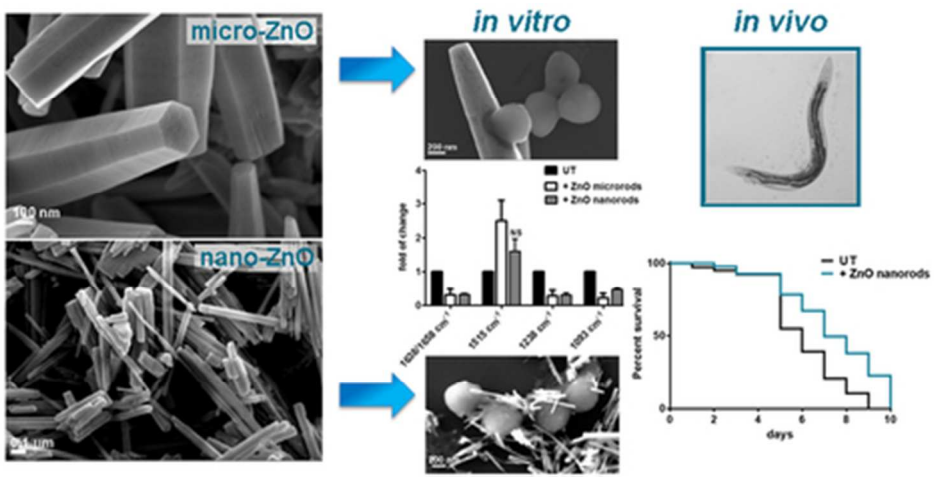

39x19mm (300 x 300 DPI)